NIH Public Access
Author Manuscript
Langmuir. Author manuscript; available in PMC 2012 November 1.

Published in final edited form as:
Langmuir. 2011 November 1; 27(21): 13104–13112. doi:10.1021/la201918y.

Characterization of poly(Sodium Styrene Sulfonate) Thin Films Grafted from Functionalized Titanium Surfaces

Gilad Zorn[1,‡], **Joe E. Baio**[1], **Tobias Weidner**[1], **Veronique Migonney**[2], and **David G. Castner**[1,*]

[1]National ESCA and Surface Analysis Center for Biomedical Problems, Departments of Chemical Engineering and Bioengineering, University of Washington, Seattle, WA 98195-1750, USA

[2]Laboratory of Biomaterials and Specialty Polymers (LBPS/CSPBAT - UMR 7244), Institut Galilée, Université Paris 13, 93430 Villetaneuse, France

Abstract

Biointegration of titanium implants in the body is controlled by their surface properties. Improving surface properties by coating with a bioactive polymer is a promising approach to improve the biological performance of titanium implants. To optimize the grafting processes, it is important to fully understand the composition and structure of the modified surfaces. The main focus of this study is to provide a detailed, multi-technique characterization of a bioactive poly(sodium styrene sulfonate) (pNaSS) thin film grafted from titanium surfaces via a two-step procedure. Thin titanium films (~50 nm thick with an average surface roughness of 0.9±0.2nm) prepared by evaporation onto silicon wafers were used as smooth model substrates. X-ray photoelectron spectroscopy (XPS) and time-of-flight secondary ion mass spectrometry (ToF-SIMS) showed that the titanium film was covered with a TiO_2 layer that was at least 10nm thick and contained hydroxyl groups present at the outermost surface. These hydroxyl groups were first modified with a 3-methacryloxypropyltrimethoxysilane (MPS) cross linker. XPS and ToF-SIMS showed that a monolayer of the MPS molecules were successfully attached onto the titanium surfaces. The pNaSS film was grafted from the MPS modified titanium through atom transfer radical polymerization. Again, XPS and ToF-SIMS were used to verify that the pNaSS molecules were successfully grafted onto the modified surfaces. Atomic force microscopy analysis showed that the film was smooth and uniformly covered the surface. Fourier transform infrared spectroscopy indicated an ordered array of grafted NaSS molecules were present on the titanium surfaces. Sum frequency generation vibration spectroscopy and near edge X-ray absorption fine structure spectroscopy illustrated that the NaSS molecules were grafted onto the titanium surface with a substantial degree of orientational order in the styrene rings.

Keywords

Titanium; Sodium Styrene Sulfonate; Surface Characterization; Silanization

Introduction

Titanium and its alloys are commonly used as biomaterials due to their unique mechanical properties and good corrosion resistance. Also, titanium is more compatible with human tissue compared to other metals[1]. These properties were the driving force for the early

*Corresponding Author: Phone 206-543-8094. castner@nb.uw.edu.
‡Current address: General Electric Global Research, One Research Circle, Niskayuna NY, 12309

NIH-PA Author Manuscript
NIH-PA Author Manuscript
NIH-PA Author Manuscript

NIH-PA Author Manuscript

NIH-PA Author Manuscript

NIH-PA Author Manuscript

introduction of cp Ti, α+β (Ti-6Al-4V), metastable β titanium alloys [2–6] and nickel titanium shape memory alloys [7]. Still, titanium implants can induce the formation of a fibrous layer that can compromise bonding at the interface with the living tissue. This lack of proper integration of titanium with tissue can lead to implant failure. Since the biological response to implanted biomaterials is influenced by the surface properties of the materials, modifying the chemical and/or physical properties of the implant's surface can be used to control the interaction between an implant and its surrounding tissue.

Over the last 10 years, many studies on surface modification of titanium and its alloys using methods such as mechanical, chemical, thermal, electrochemical and biochemical treatments have been published [3,5,8–13]. A promising simple approach to surface modification is grafting a bioactive polymer from titanium implant surfaces[2]. It has already been shown that polymers bearing appropriate chemical functions can modulate cell attachment, spreading and activity on these bioactive polymers [14,15]. Atom transfer radical polymerization (ATRP) is a recently developed radical polymerization method which does not require stringent experimental conditions [16–18]. It is an effective method of grafting polymers from solid surfaces such as gold [19–21], silicon [22–24], glass [25,26], stainless steel [27] and titanium [27–31] It allows the direct polymerization of wide range of functional monomers in a controlled fashion with narrowly dispersed molecular weight [17,18,31]. Grafting of ionic polymers such as poly(sodium styrene sulfonate) (pNaSS) by ATRP from titanium surfaces create active sites due to the distributions of ionic groups along the macromolecular chains. These active sites can interact with extracellular proteins, such as fibronectin, implicated in cell response[2,14,15].

We previously described the optimization of a grafting procedure to produce a uniform layer of bioactive pNaSS on titanium surfaces [32]. The next step is to obtain a detailed characterization of the modified surfaces. Properties such as film thickness, uniformity, degree of order and orientation have a pivotal role in the biomaterial performance and therefore should be quantitatively analyzed. Hence we have performed a rigorous analytical study to understand the elemental composition, molecular structure and orientation of the grafted pNaSS films. Our detailed multi-technique study was performed by using smooth titanium films evaporated onto flat silicon wafers as a model system [4,33]. NaSS molecules were grafted from the titanium surfaces employing the two-step procedure shown in Figure 1. First the titanium surfaces were modified by attaching a monolayer of 3-methacryloxypropyltrimethoxysilane (MPS) cross-linker molecules. Then NaSS monomers were grafted from the modified surface using ATRP to covalently bind the methacrylate tails of the silane cross linkers to the carbon double bond (C=C) of the NaSS units. Quantitative surface elemental compositions at each step in the grafting process were determined with X-ray photoelectron spectroscopy (XPS). Time-of-flight secondary ion mass spectrometry (ToF-SIMS) provided molecular structure information about the MPS and pNaSS layers as well as an evidence for the covalent grafting of pNaSS to the modified titanium surface. Atomic force microscopy (AFM) was used to quantify the surface roughness and uniformity of the pNaSS grafted films. Finally, Fourier transform infrared spectroscopy (FTIR), sum frequency generation (SFG) vibrational spectroscopy and near edge X-ray absorption fine structure (NEXAFS) spectroscopy were used to provide further details about the molecular order in the MPS and pNaSS films. FTIR, SFG and NEXAFS indicate a substantial degree of ordering of the grafted pNaSS where the styrene rings are perpendicular to the titanium surface. This comprehensive surface characterization of the grafted pNaSS films provided complementary information about the composition, structure and orientation of the pNaSS layers and it is shown that a robust, uniform and ordered pNaSS film was covalently grafted from the modified titanium surface.

NIH-PA Author Manuscript

NIH-PA Author Manuscript

NIH-PA Author Manuscript

Materials and Methods

Materials

The substrates used in this study were 1×0.6 cm^2 pieces cut from a silicon wafer (Silicon Valley Microelectronics, Inc., San Jose), then coated with ~50 nm of titanium by electron beam evaporation at pressures below 1×10^{-6} torr. 3-methacryloxypropyltrimethoxysilane (MPS) was purchased from Gelest Inc. Sodium styrene sulfonate (NaSS), azobisisobutyronitrile (AIBN), chloroform ($CHCl_3$) and dimethyl sulfoxide (DMSO) were purchased from Sigma. NaSS was purified by dissolving it in a mixture of water/ethanol (10/90 v/v) at 70°C and then recrystallizing under vacuum[15]. AIBN was purified by dissolving it in methanol, recrystallizing at −18°C and drying under vacuum.

Silanization and pNaSS grafting

The titanium substrates were sonicated in $CHCl_3$ for 15mins and then soaked in a $CHCl_3$ solution of MPS (5%v/v) for 1 hour[25,34]. The samples were then gently rinsed in $CHCl_3$ and followed by heating at 140° C for 4 hours[25]. Finally the samples were sonicated in $CHCl_3$ for 30 minutes and then were air dried. After drying, the samples were immersed in a DMSO solution of 0.7M NaSS monomer[2,14,15] and 9×10^{-3} M AIBN. The solution was degassed for 2 hours to create an oxygen-free atmosphere and then heated to 90° C for 15 hours under vacuum. The samples were then finally rinsed in deionized (DI) water, sonicated for 15 minutes in DI water[2] and dried under vacuum.

X-ray Photoelectron Spectroscopy

XPS measurements were performed on a Kratos AXIS Ultra DLD instrument (Kratos, Manchester, England) in the hybrid mode (the hybrid mode detects a wide range of photoelectron take-off angles) using a monochromatic Al Kα X-ray source. Compositional survey scans were acquired at a nominal photoelectron take-off angle of 0° (the photoelectron take-off angle is the angle between the surface normal of the sample and the axis of the analyzer lens) using an analyzer pass energy of 80 eV and high-resolution spectra were acquired using an analyzer pass energy of 20 eV. All binding energies (BEs) were referenced to the hydrocarbon C 1s peak at 285 eV. Three spots on two or more replicates of each sample type were analyzed. The compositional data are an average of the values determined at each spot. Compositions were calculated with the CasaXPS software and high-resolution peaks were fit with the XPSPEAK 4.1 software.

Time of Flight Secondary Ions Spectroscopy

ToF-SIMS experiments were performed using an ION-TOF TOF.SIMS 5–100 (ION-TOF GmbH, Münster, Germany). A liquid metal ion gun (LMIG) was used to generate the pulsed 25 kV Bi_3^+ beam. The analysis Bi_3^+ beam was rastered over a 100 × 100 μm^2 area on the sample surface and the total ion dose used to acquire each spectrum was less than 1×10^{12} ions/cm^2. The mass resolution (m/Δm) was above 7500 for all mass spectra. The mass scales of the positive secondary ion spectra were calibrated using the CH_3^+, $C_2H_3^+$, $C_2H_5^+$ and $C_3H_5^+$ peaks. The mass scales of the negative secondary ion spectra were calibrated using the CH^-, O^-, OH^-, and C_2H^- peaks. At least two replicates were analyzed for each sample type with five spectra acquired at five different spots on each replicate. Data analysis was performed using IonSpec data reduction software from ION-TOF GmbH. Peak intensities were normalized using the total intensity for each spectrum.

Atomic Force Microscopy (AFM)

The surface morphologies and roughness were measured using AFM (Dimension 3100, Veeco Metrology Inc., Santa Barbara, CA). The AFM was equipped with a 315 kHz, 42 N/

NIH-PA Author Manuscript

NIH-PA Author Manuscript

NIH-PA Author Manuscript

m PointProbe Plus silicon tip (Nanosensors, Neuchatel, Switzerland) and operated in the intermittent contact mode in air. At least three locations on the sample were scanned to determine the average roughness over a 400 μm^2 area.

Fourier Transform Infrared Spectroscopy (FTIR)

FTIR measurements were performed using a Bruker Tensor spectrometer with a germanium attenuated total reflectance (ATR) crystal in the mid-IR frequency range (4000 – 400 cm^{-1}). A spectrum was acquired with 1000 scans at 4 cm^{-1} resolution and the data were analyzed using the OPUS software.

Sun Frequency Generation (SFG)

SFG spectra were acquired with an EKSPLA instrument (EKSPLA, Vilnius, Lithuania) by overlapping visible and tunable IR laser pulses (25 ps) in time and space at incidence angles of 60° and 54°, respectively. Details of the instrumentation setup are published elsewhere[35]. Briefly, the visible beam with a wavelength of 532 nm was generated by an EKSPLA Nd:YAG laser operating at 50 Hz, which was also used to pump an EKSPLA optical parametric generation/amplification and difference frequency unit based on barium borate and $AgGaS_2$ crystals to generate tunable IR laser radiation from 1000–4000 cm^{-1}. The bandwidth was 1 cm^{-1} for the visible pump pulses and 1 cm^{-1} for the IR laser radiation, which is significantly less than the spectral features examined in this study. Both beams were mildly focused and had a diameter of approximately 1 mm at the sample. The energy for both beams was 160 μJ per pulse. The spectra were collected with 200 shots per data point in 4 cm^{-1} increments and the final spectra were obtained by averaging over at least four spectra. All spectra were recorded in the *ppp* (sum, visible, and infrared) polarization combination and were normalized by a reference SFG signal generated in a ZnS crystal. SFG is a coherent non-linear optical process where spectrally tunable infrared and fixed visible laser pulses are overlapped in time and space at an interface and generate photons at the sum of the pump beam frequencies.

The intensity of the generated SF light I is given by[36,37]:

$$I_{SF} \propto \left|\chi^{(2)}_{eff}\right|^2 I_{IR}\, I_{vis} \tag{1}$$

here, I_{vis} and I_{IR} are the infrared and visible pump beam intensities, respectively, and $\chi^{(2)}_{eff}$ denotes the effective second-order nonlinear susceptibility of the interface which can be written as[38]:

$$I_{SFG} \propto \left|\chi^{(2)}\right|^2 = \left|\chi^{(2)}_{NR} + \sum_{\nu} \frac{A_\nu e^{i\varphi_\nu}}{\omega_{IR} - \omega_\nu + i\Gamma_\nu}\right|^2 \tag{2}$$

Here, $\chi^{(2)}_{NR}$ is the second order nonlinear susceptibility of the non-resonant background, A_ν is the strength of the ν^{th} vibrational mode, φ_ν denotes the phase of the respective mode and ω_{IR} refers to the frequency of the incident IR field. ω_ν and Γ_ν are the resonance position and width of the respective modes, respectively. Fitting eq 2 to the spectral data allows us to determine A_ν, ω_ν and Γ_ν. In the fits, the Lorentzian line widths were set to 2 cm^{-1} and Γ_ν was allowed to vary since the two contributions to the total line width could not be separated within the accuracy of the measurements.

NIH-PA Author Manuscript

NIH-PA Author Manuscript

NIH-PA Author Manuscript

Near Edge X-ray absorption fine structures (NEXAFS)

NEXAFS spectra were collected at the U7A beamline at the National Synchrotron Light Source (NSLS, Brookhaven National Laboratory, Upton, NY) using an elliptically ~ 85% p-polarized beam. The beam line is equipped with a monochromator and a 600 l/mm grating that provides a full-width at half maximum resolution of ~ 0.15 eV at the carbon K-edge (285 eV). The monochromator energy scale was calibrated using the 285.35 eV C 1s to π* transition on a graphite transmission grid[39] and partial electron yields were divided by the beam flux during data acquisition[40]. A detector with a bias voltage set at − 250 V for the C K-edge was used to monitor the partial electron yield. All samples were mounted to allow rotation about the vertical axis, thus, allowing the NEXAFS angle, the angle between the incident X-ray beam and the sample surface, to be varied. All spectra were normalized to an edge step height of unity.

Results and discussion

1. Characterization of the evaporated titanium surface

Surface characterization (composition, thickness, coverage), in general, is most straightforward to do on, flat substrates[4] Orientational studies, in particular, must be performed on smooth, uniform surfaces Thus, ~50nm thick titanium layers were deposited onto silicon wafers by e-beam evaporation. This well-defined and reproducible process provided smooth, flat titanium surfaces with comparable surface compositions to commercially available pure Ti foil [32]. The AFM image of the evaporated film showed that these surfaces had an average roughness of 0.9±0.2nm (Figure 2a). The XPS determined elemental composition for the evaporated titanium surfaces is shown in Table 1. As expected, ~30 at% carbon was detected due to the presence of adventitious organic contamination on the titanium surface[4]. The high-resolution O1s line shape (Table S1 in Supporting Information and Figure 3a) was fit to two components at 530.2 eV (TiO_2) and 531.8 eV (surface hydroxide groups as well as adsorbed water and surface contamination) [41–43]. In addition, the high-resolution Ti2p line shape and BEs (Figure 3f) are consistent with the presence of TiO_2. $Ti_xO_yH_z$ fragments were detected from the titanium surface in ToF-SIMS positive and negative secondary ion spectra (Tables S2 and S3 in Supporting Information). In addition positive Ti_xO_y secondary ions (Table S3) were detected. The oxidized titanium species observed by ToF-SIMS are consistent with the XPS results and verifies the presence of hydroxide groups on the evaporated surfaces, which are essential for surface silanization[3,44].

2. Modification of the Titanium surfaces by MPS Silanization

Siloxane-anchored thin films are known to interact strongly with hydroxylated surfaces of substrates such as silicon oxide, aluminum oxide, glass, mica and titanium oxides[45]. The driving force for the silanization is the in-situ formation of a polysiloxane network. To limit the silanization process to a monolayer and achieve covalent attachment of the polysiloxane network to the surface requires careful control of the water concentration in the silane solution.[46] Silane chemistry has been widely been used to graft polymer brushes such as styrene, acrylates and poly(ethylene glycol) from silicon, glass and titanium oxide surfaces thorough ATRP [22,23,25,26,31,47]. In this study MPS molecules were used as a cross linkers for the NaSS molecules and it was essential to fully determine the characteristics of modified surface before grafting the pNaSS. To confirm that a uniform monolayer is formed requires detailed characterization with techniques such as XPS and ToF-SIMS[48], FTIR and SFG. After attaching the MPS molecules onto the titanium surfaces, XPS detected the presence of Si from the MPS trimethoxysilane tails (Table 1). Moreover, similar to other studies of organic overlays on solid surfaces, the XPS elemental composition can provide an insight about the chemical composition of the film [4,35,49,50]. The carbon to silicon ratio in

NIH-PA Author Manuscript

NIH-PA Author Manuscript

NIH-PA Author Manuscript

Table 1 is 9.4±0.2, which is slightly higher than the theoretical value of 7 expected for a fully hydrolyzed and crosslinked MPS molecule (i.e., elimination of all methyl groups from all three methoxy species in the starting MPS molecule). These results are consistent with the surface contaminants present on the evaporated titanium being displaced by MPS molecules during the silanization process. The slightly larger experimental value indicates either all the methoxy groups were not hydrolyzed or the presence of some adventitious hydrocarbon species or organic solvent residues on the MPS modified titanium surfaces. The high-resolution O1s XPS peak from the MPS modified titanium (Table S1 and Figure 3b), was fit with three components at 530.2, 531.8 and 533.1 eV. Similar to the evaporated Ti, the peak at 530.2 eV is assigned to TiO_2 while the peaks at 531.8 and 533.1 eV are associated with the MPS molecules. The ratio between the titanium and the oxygen peak at 530.2 is 0.4, while the ratio between the carbon and the two oxygen peaks at 531.8 and 533.1 eV (assigned to MPS) is 1.9. The Ti/O ratio is in good agreement with the theoretical values of 0.5 expected for TiO_2. The C/O ratio is higher than the theoretical value of 1.4 expected for fully hydrolyzed and crosslinked MPS, consistent with the C/Si XPS results. The C1s high-resolution XPS peak from the MPS modified titanium (Table S1 and Figure 3b) was fit into three components at 285 eV (C-C and C-H), 286.5eV (CO-C and C-O-Si) and 288.9 (O-C=O). The carbon-oxygen species can be attributed to the methacrylate group, while the C-O-Si species could originate from unreacted methoxy groups.

To gain further insight into the bonding of the MPS to the Ti surface, ToF-SIMS analysis was done (Tables S2 and S3). The main ToF-SIMS fragments detected from the MPS modified titanium surface were SiO_xCH_y ions originating from the MPS trimethoxysilane tail group and $C_xH_yO_z$ ions originating from the MPS methacrylate head group. In addition, small $TiSiO_xCH_y$ fragments were detected, which are consistent with covalent bonding between the MPS methoxysilane tails and the titanium surface shown in Figure 1.

Orientational studies of the MPS films were performed with FTIR and SFG. The C-H region in the FTIR spectrum of the MPS modified titanium is presented in Figure 4a. Asymmetric C-H stretches of 2920 cm^{-1} and symmetric C-H stretches of 2850 cm^{-1} suggests that the MPS molecules form an ordered film on top of the titanium surface[51]. An SFG spectrum of the MPS modified titanium surface in the C-H stretching region is shown in Figure 5 along with the corresponding fits of Eqn. 2. This spectrum has C-H stretching resonances for the methylene groups near 2865 cm^{-1} (d^+) and 2920 cm^{-1} (d^-) and strong modes related to the methacrylate methyl groups near 2880 cm^{-1} (r^+: symmetric stretch), 2935 cm^{-1} (r^+_{Fermi}: Fermi resonance) and 2965 cm^{-1} (r^-: asymmetric stretch) [52–55]. Well ordered methylene chains with even numbers of CH_2 groups and all-trans conformations do not generate an SFG signal because of the inversion symmetry presence in such chains[53]. The methylene modes observed in Figure 5 indicate either gauche defects in the MPS film or a partial loss of the inversion symmetry due to the odd number of methylene groups in the MPS chain. The reasonable intensity of the methyl modes in the spectra indicates a reasonable degree of order of the MPS film, and is in good agreement with the FTIR data.

The tilt angles Θ of the methyl units relative to the surface normal can be estimated based on the intensities *A* observed for the methyl r^+ and r^- modes [56]:

$$\frac{A_{r^-}}{A_{r^+}} = D\frac{\langle \cos\Theta - \cos 3\Theta \rangle}{\cos\Theta} \quad (3)$$

where *D* is the proportionality constant which includes the hyperpolarizability and Fresnel factors of the terminal methyl group. The brackets stand for a distribution function for the tilt angles. Detailed information about this analysis has been published elsewhere [56,57]. For

NIH-PA Author Manuscript

NIH-PA Author Manuscript

NIH-PA Author Manuscript

simplicity, a uniform orientation of all MPS chains was assumed to provide an estimate of the molecular orientation. Nishi et al. have experimentally determined the constant D to be 3.5 for aliphatic monolayers.[56] This analysis yields a tilt angle of 15° for the methyl—propenoate β-carbon bond *vs*. the surface normal.

3. Grafting pNaSS onto the surface of the MPS modified Titanium

The aim of the present study was to fully characterize and obtain a detailed insight about the structure, composition and orientation of grafted pNaSS onto titanium surface. The pNaSS film was grafted from the MPS modified titanium by ATRP [16–32,47]. The XPS surface composition of pNaSS grafted titanium surface (Table 1) exhibited an increased carbon signal as well as decreased titanium and oxygen signals as compared to the MPS modified titanium surface. This is consistent with the fact that pNaSS contains mainly carbon and forms an overlayer film on top of the MPS modified titanium. As a control experiment, the AIBN initiator was omitted from the reaction, resulting in a surface that had a significantly lower carbon (38.9±0.4 vs 51.1±0.6 atomic %) sulfur (1.3±0.2 vs. 3.3±0.1 atomic %) and nitrogen (not detected vs. 1.1±0.1 atomic %) concentrations, as well as significantly higher titanium (12.7±0.5 vs. 8.4±0.2 atomic %) and oxygen (42.4±0.2 vs. 32.6±0.7 atomic %) concentrations. The XPS results are consistent with the grafting several NaSS monomers (see Figure 1). The number of NaSS monomers grafted from the surface will depend on the exact tilt and twist angles of the polymer backbone and side chains.

In addition, XPS detected the presence of sulfur and sodium, which are unique to pNaSS, providing further evidence of the successful grafting of pNaSS to the MPS modified surface. The nitrogen signal detected by XPS is likely due to some residual AIBN species remaining in the pNaSS film. This is consistent with the presence of nitrogen containing fragments in both negative (Table S2) and positive (Table S3) ToF-SIMS data. The high-resolution XPS O1s spectrum shows an increase in the peak at 531.8 eV (Table S1 and Figure 3c) assigned to species with an oxygen double bond. Its intensity increase can be explained by the contribution of the S=O groups present in the pNaSS film. The high resolution C1s shows an increase in the hydrocarbon peak at 285.0 eV (Table S1 and Figure 3e). This peak accounts for ~ 90% of the carbon signal, consistent with the fact that 7 of 8 carbons in pNaSS are hydrocarbon species.

Negative secondary ion fragments from the ToF-SIMS experiments (Table S2) provide direct evidence for the presence of pNaSS in the grafted films. SO_x, $C_yH_zSO_x$, and $C_yH_zSO_xNa$ fragments are all directly related to the structure of pNaSS (see Figure 1). In particular, the strong intensity of $C_8H_7SO_3$ fragment (NaSS monomer) indicates the presence of NaSS on the titanium surface. ToF-SIMS also detected fragments ($C_8H_{10}SO_3$-$C_4H_5O_2$ and $C_8H_{10}SO_3$-$C_2H_3O_2$-C_3H_z) that were consistent with covalent attachment of NaSS to MPS. In addition, the fragments originating from two NaSS units ($C_{15}H_zO_6S_2$, $C_8H_{10}SO_3$-C_8H_4-$C_2H_3O_2$-C_yH_z and $C_{12}H_zO_x$) were detected, consistent with polymerization of the NaSS monomers in the grafted film. The presence of the fragments originating from multiple NaSS monomers in the grafted layer is consistent with the XPS results. The ToF-SIMS intensities of the titanium containing fragments and the MPS fragments decreased after pNaSS grafting (Tables S2 and S3). Similar to the XPS analysis, this observation is explained by the fact that the pNaSS film forms an overlayer film on top of the MPS modified titanium surface.

AFM analysis of the pNaSS grafted titanium (Figure 2b) shows that the grafted pNaSS film uniformly covers the titanium surface. The grafted layer closely mimics the topography of the substrate and there is little apparent influence of the grafted pNaSS on the overall morphology. The AFM determined roughness for the pNaSS grafted surfaces, 1.4±0.2nm, is

NIH-PA Author Manuscript

NIH-PA Author Manuscript

NIH-PA Author Manuscript

similar to the roughness of the as evaporated titanium surface before MPS modification and pNaSS grafting.

Our smooth, clean evaporated titanium surface allows us to study in detail the orientation and order of the pNaSS film. The C-H region in the FTIR spectrum of the pNaSS grafted titanium (Figure 4a) presents asymmetric C-H stretching of 2920 cm^{-1} and symmetric C-H stretches of 2850 cm^{-1}. Similar to the MPS film, these values indicate that the grafted film forms an ordered film on the titanium surfaces, in line with the SFG results. The finger print region in the FTIR spectrum (Figure 4b) exhibits two characteristic peaks at 1008 and 1036 cm^{-1} from the sulfonate group[2]. The SFG spectrum for the pNaSS grafted titanium (Figure 5) shows a spectral feature near 3050 cm^{-1} related to the ν_{7a} mode of the styrene ring. This further supports the XPS and ToF-SIMS results, which showed the pNaSS was successfully grafted onto the titanium surfaces. The presence of this mode in the SFG spectrum indicates a substantial degree of ordering of the styrene rings. Based on Eqn (3), the tilt angles Θ of the methyl units was estimated as 26° (relative to the surface normal) for the pNaSS grafted film.

Changes of the MPS film structure upon pNaSS grafting can be monitored semi-quantitatively by analyzing intensity changes in the methyl and methylene modes. It should be noted that determining of the exact MPS+pNaSS film orientation requires a consideration of the twist angle (i.e. the rotation with respect to molecular axis). The twist angle of the MPS film is unknown, but a general trend can be estimated. The methacrylate methyl group is oriented perpendicular to the MPS chain and along to the pNaSS-MPS bond. Considering the molecular architecture, our results indicate a more upright orientation of the methacrylate moiety upon pNaSS grafting. In addition, the strength of the methylene modes can be used to study changes in the chain conformation. The intensity of the d^+ mode correlates with conformational disorder in hydrocarbon chains. The methylene signal normalized to the intensity of the methyl resonances provides a quantitative estimation of the chain order that is independent of the surface density[58]. The r^+/d^+ ratios are 4.6 and 2.1 for the MPS film before and after pNaSS grafting, respectively. There are three methylenes in the chain and the 45% increase of the r^+/d^+ ratio indicates that, on average, an additional gauche defect is created due to the pNaSS grafting.

NEXAFS spectra provide complementary information about the electronic and chemical structure of the grafted pNaSS. In particular they provide detailed information about the orientation of the styrene ring with respect to the titanium surface. NEXAFS exhibit characteristic absorption resonances corresponding with the electronic transition from a given core level to unoccupied molecular orbitals[40] which can be used to probe surface chemistry and to detect the molecular orientation on surfaces. As the first step in NEXAFS analysis, the carbon K-edge spectra for evaporated titanium, MPS modified titanium and pNaSS grafted titanium surfaces are presented in Figure 6a. These spectra were acquired at a NEXAFS angle of 55° which is the “magic angle” for NEXAFS and is typically used to compare differences in bonding features among samples[40]. All three spectra exhibit a characteristic resonance near 285 eV, related to the π* resonance from C-C bonds within the ethylene and styrene groups and two broad peaks near 289 and 298eV[59,60]. These broad peaks correspond to σ* transitions from the C-C, C=C, C-O, and C=O bonds within the MPS[61]. Examining the spectra from each step of the surface grafting process, two clear changes in the spectra are observed. A large increase in intensity of the π* resonance at 285eV corresponding to the C-C bonds within the styrene ring structure and a small drop in intensity of the σ* transition at 289 eV occurs after pNaSS grafting [59,60].

The second and final step in the NEXAFS analysis is to examine the dependence of the styrene π* resonance intensity on the incident angle of X-ray light (i.e. the linear dichroism).

NIH-PA Author Manuscript

NIH-PA Author Manuscript

NIH-PA Author Manuscript

In addition to FTIR and SFG, this unique analysis provides complementary information about the orientation of the pNaSS on the titanium surface. A convenient way to monitor the linear dichroism is to measure the difference between the spectra acquired at different incidence angles (i.e., 70°-20°). Such difference spectra (Figure 6b) illustrate that the characteristic π* resonances vary with changing X-ray incident angle. From this large positive dichroism, average tilt angles of the π* orbitals were calculated by assuming the π* orbitals point in a specific direction (vector type)[62]. The π* orbitals were assumed to be oriented perpendicular to the plane of the styrene ring. This produced an average styrene ring tilt angle of 25 ± 3° with respect to normal of the titanium surface.

Conclusions

A two-step procedure was developed to graft bioactive pNaSS thin films from titanium surfaces. A complementary study with XPS, ToF-SIMS, AFM, FTIR, SFG and NEXAFS provides a detailed understanding of the titanium surface at each step in the procedure.

Smooth titanium films (mean square roughness of 0.9nm) evaporated onto silicon wafers were used as substrates in this study. These model substrates were used to perform a detailed complementary study of the chemical composition, molecular structure and orientation of the grafted pNaSS films. XPS and ToF-SIMS showed the chemical state of the Ti substrates were TiO_2 and hydroxide groups were present at their topmost surfaces. MPS molecules were used as a cross linker between the titanium surface and the pNaSS film. After attaching the MPS molecules to the titanium surfaces, XPS data suggested that the titanium substrates were covered by a uniform MPS monolayer. Additional evidence for the MPS attachment to the titanium surfaces was the appearance of the ToF-SIMS fragments from MPS and MPS plus titanium along with the decrease of the ToF-SIMS fragments from the titanium surface.

After pNaSS grafting, the XPS composition showed an increase of the carbon to titanium ratio and the appearance of sulfur and sodium, consistent with polymerization of several NaSS monomers. ToF-SIMS successfully detected fragments from NaSS in the grafted film along with a decrease in titanium containing fragments. AFM analysis of the pNaSS grafted surface showed a uniform coverage with a roughness of 1.4nm. Finally, FTIR, SFG and NEXAFS indicate an ordered array of grafted pNaSS on the titanium surfaces and show that the pNaSS is grafted with a substantial degree of orientational order in the styrene rings.

Supplementary Material

Refer to Web version on PubMed Central for supplementary material.

Acknowledgments

This research was supported by NIH grant EB-002027 (NESAC/Bio) from the National Institute on Biomedical Imaging and Bioengineering. T.W. thanks the Deutsche Forschungsgemeinschaft for a research fellowship (We 4478/1-1). The AFM studies were conducted at the University of Washington NanoTech User Facility, a member of the NSF National Nanotechnology Infrastructure Network (NNIN). We also thank Daniel Fischer and Cherno Jaye (NIST) for their help at NSLS. The NEXAFS studies were performed at the NSLS, Brookhaven National Laboratory, which is supported by the U.S. Department of Energy, Division of Materials Science and Division of Chemical Sciences.

References

1. Leventhal GS. Journal of Bone and Joint Surgery. 1951; 33-A:473. [PubMed: 14824196]
2. Helary G, Noirclere F, Mayingi J, Migonney V. Acta Biomaterials. 2009; 5:124–133.
3. Schwartz Z, Avaltroni MJ, Danahy MP, Silverman BM, Hanson EL, Schwarzbauer JE, Midwood KS, Gawalt ES. Material Science and Engineering C. 2003; 23:395–400.

NIH-PA Author Manuscript

NIH-PA Author Manuscript

NIH-PA Author Manuscript

4. Zorn G, Gotman I, Gutmanas EY, Adadi R, Salitra G, Sukenik CN. Chemistry of Materials. 2005; 17:4218–1226.
5. Zorn G, Gotman I, Gutmanas EY, Adadi R, Sukenik CN. Journal of Marterials Science: Materials in Medicine. 2007; 18:1309–1315.
6. Noort VR. Journal of Materials Science. 1987; 22:3801–3811.
7. Shabalovskaya SA. International Materials Reviews. 2001; 46:233–250.
8. Puleo DA, Nanci A. Biomaterials. 1999; 20:2311–2321. [PubMed: 10614937]
9. Xiao SJ, Textor M, Spencer ND. Langmuir. 1998; 14:5507–5516.
10. Lausmaa J, Kasemo B, Mattasson H, Odelius H. Applied Surface Science. 1990; 45:189.
11. Nanci A, Wuest JD, Peru L, Brunet P, Sharma V, Zalzal S, McKee MD. Journal of Biomedical Materials Reserch. 1998:40.
12. Matinlinna JP, Laajalehto K, Lahito T, Kangasniemi I, Lassila LVJ, Vallittu PK. Surface and Interface Analysis. 2004; 36:246–253.
13. Michiardi A, Hélary G, Nguyen PCT, Gamble LJ, Anagnostou F, Castner DG, Migonney V. Acta Biomaterialia. 2010; 6:667–675. [PubMed: 19733698]
14. Djavid-Pavon G, Gamble LJ, Ciobanu M, Gueguen V, Castner DG, Migonney V. Biomacromolecules. 2007; 8:3317–3325. [PubMed: 17929865]
15. Ciobanu M, Siove A, Gueguen V, Gamble LJ, Castner DG, Migonney V. Biomacromolecules. 2006; 7:755–760. [PubMed: 16529411]
16. Eckenhoff TW, Pintauer T. Inorganic Chemistry. 2007; 46:5844–5846. [PubMed: 17602555]
17. Matyjaszewski K, Dong H, Jakubowski W, Pietrasik J, Kusomo A. Langmuir. 2007; 23:4528–4531. [PubMed: 17371060]
18. Oh JK, Min K, Matyjaszewski K. Macromolecules. 2006; 39:3161–3167.
19. Gopireddy D, Husson SM. Macromolecules. 2002; 35:4218–4221.
20. Jordan R, Ulman A, Kang JF, Rafailovich MH, Sokolov J. Journal of the American Chemical Society. 1999; 121:1016–1022.
21. Ma H, Li D, Sheng X, Zhao B, Chilkoti A. Langmuir. 2006; 22:3571–3576.
22. Biesalski M, Rühe J. Langmuir. 2000; 16:1943–1950.
23. Prucker O, Rühe J. Macromolecules. 1998; 31:602–613.
24. Sidorenko A, Minko S, Schenk-Meuser K, Duschner H, Stamm M. Langmuir. 1999; 15:8349–8355.
25. Hucknall A, Kim DH, Rangarajan S, Hill RT, Reichert WM, Chilkoti A. Advanced Materials. 2009; 21:1968–1971.
26. Prucker O, Rühe J. Macromolecules. 1999; 32:2309–2316.
27. Fan X, Lin L, Dalsin JL, Messersmith PB. Journal of the American Chemical Society. 2005; 127:15843–15847. [PubMed: 16277527]
28. Barthélémy B, Devillers S, Minet I, Delhalle J, Mekhalis Z. journal of Colloid and Interface Science. 2011; 354:873–879. [PubMed: 21168144]
29. Fan X, Lin L, Messersmith PB. Biomacromolecules. 2006; 7:2443–2448. [PubMed: 16903694]
30. Kang SM, Lee BS, Kim WJ, Choi IS, Kil M, Jung HJ, Oh E. Macromolecular Research. 2009; 17:174–180.
31. Zhang F, Xu FJ, Kang ET, Neoh KG. Ind Eng Chem Res. 2006; 45:3067–3073.
32. Libey TG, Zorn G, Castner DG. Journal of Undergraduate Research in Bioengineering. 2008–2010; 8:72–76.
33. Adadi R, Zorn G, Brener R, Gotman I, Gutmanas EY, Sukenik CN. Thin Solid Films. 2010; 518:1966–1972.
34. Hull JR, Shannon JJ, Tamura GS, Castner DG. Biointerphases. 2007; 2:64–72. [PubMed: 20408638]
35. Baio JE, Weidner T, Brison J, Graham DJ, Gamble LJ, Castner DG. Journal of Electron Spectroscopy and Related Phenomena. 2009; 172:2–8. [PubMed: 20161353]
36. Boyd, RW. Nonlinear Optics. 1. Academic Press; London: 1992.

NIH-PA Author Manuscript

NIH-PA Author Manuscript

NIH-PA Author Manuscript

37. Shen, YR. The Principles of Nonlinear Optics. 1. John Wiley & Sons; New York: 1984.
38. Bain CD, Davies PB, Ong TH, Ward RN, Brown MA. Langmuir. 1991; 7:1563–1566.
39. Baston PE. Physical Review B. 1993; 48:2680.
40. Stöhr, J. NEXAFS Spectroscopy. Vol. 25. Springer-Verlag; Berlin: 1992.
41. Zorn G, Adadi R, Brener R, Yakovlev VA, Gotman I, Gutmanas EY, Sukenik CN. Chemistry of Materials. 2008; 20:5368–5374.
42. Textor M, Ruiz L, Hofer R, Rossi A, Feldman K, Hahner G, Spencer ND. Langmuir. 2000; 16:3257–3271.
43. Ratner, BD.; Castner, DG. Electron Spectroscopy for Chemical Analysis. In: Vickerman, JC.; Gilmore, IS., editors. Surface Analysis The Principle Techniques. 2. Wiley; New York: 2009. p. 47
44. Silverman BM, Wieghaus KA, Schwartz J. Langmuir. 2005:21.
45. Ulman A. Chemical Reviews. 1996; 96:1533–1554. [PubMed: 11848802]
46. Tripp CP, Hair ML. Langmuir. 1992; 8:1120–1126.
47. Matyjaszewski K, Miller PJ, Shukla N, Immaraporn B, Gelman A, Luokala BB, Siclovan TM, Kickelbick G, Vallant T, Hoffmann H, Pakula T. Macromolecules. 1999; 32:8716–8724.
48. Mao G, Castner DG, Grainger DW. Chemistry of Materials. 1997; 9:1741–1750.
49. Cheng F, Gamble LJ, Castner DG. Analytical Chemistry. 2008; 80:2564–2573. [PubMed: 18302347]
50. Techane SD, Gamble LJ, Castner DG. Journal of Physical Chemistry C. 2011; 115:9432–9441.
51. Nuzzo RG, Dubois LH, Allara DL. Journal of the American Chemical Society. 1990; 112:558–569.
52. Briggman KA, Stephenson JC, Wallace WE, Richter LJ. Journal of Physical Chemistry B. 2001; 105:2785–2791.
53. Himmelhaus M, Eisert F, Buck M, Grunze M. Journal of Physical Chemistry B. 2000; 104:576–584.
54. Bellamy, LD. The infra-red spectra of complex molecules. 3. Lowe & Brydone; Thetford, Norfolk: 1975.
55. Varsanyi, G. Adam Hilger. Vol. 1.1, 1.2, 2. London: 1974.
56. Nishi N, Hobara D, Yamamoto M, Kakiuchi T. Journal of Chemical Physics. 2003; 118:1904–1911.
57. Zhang H, Romero C, Baldelli S. Journal of Physical Chemistry B. 2005; 109:15520–15530.
58. Bell GR, Bain CD, Ward RN. Journal of the Chemical Soceity, Faraday Transactions. 1996; 92:515–523.
59. Liu AC, Stöhr J, Friend CM, Madix RJ. Surface Science. 1990; 235:107–115.
60. Horsley JA, Stöhr J, Hitchcock AP, Newbury DC, Johnson AL, Sette F. Journal of Chemical Physics. 1985; 83:6099–6107.
61. Outka DA, Stöhr J, Madix RJ. Surface Science. 1987; 185:53–74.
62. Stöhr J, Outka DA. Physical Review B. 1987; 36:7891–7905.

NIH-PA Author Manuscript

NIH-PA Author Manuscript

NIH-PA Author Manuscript

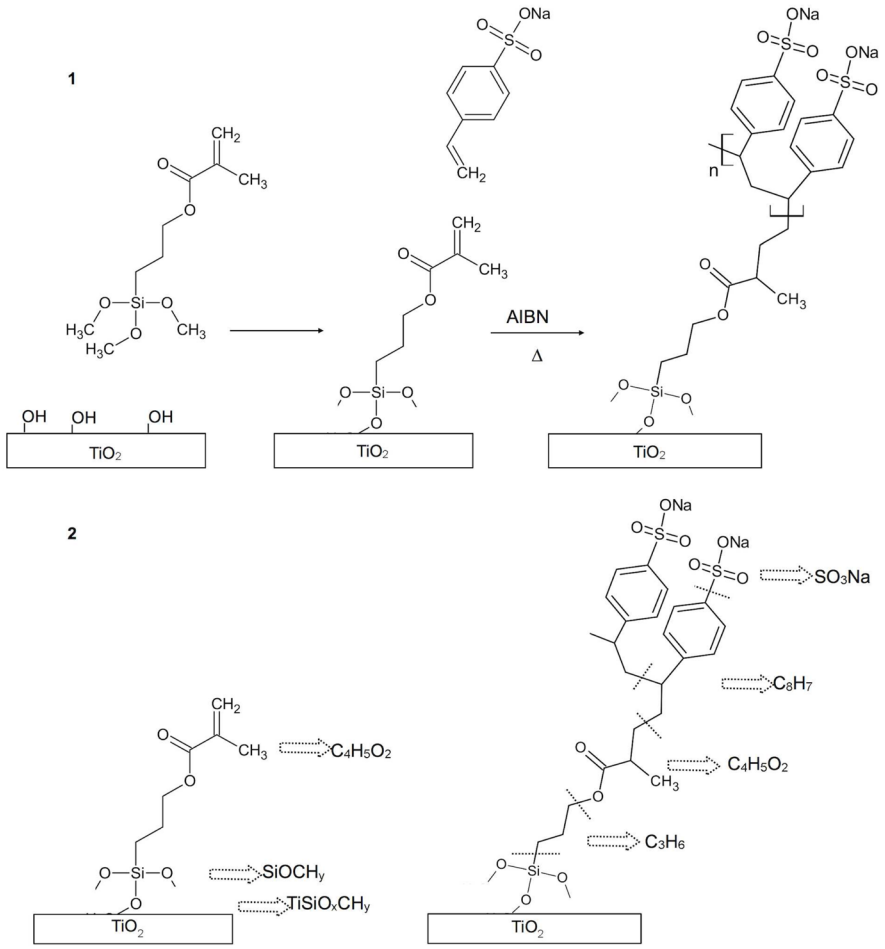

Figure 1.

(1) A schematic drawing of the two-step pNaSS grafting procedure: first surface modification by attaching a monolayer of MPS molecules and then pNaSS grafting from the modified surface using ATRP (the methacrylate tails of the silane cross linkers covalently bond to the carbon double bond (C=C) of the NaSS monomers. (2) Key ToF-SIMS fragments are noted for each step.

NIH-PA Author Manuscript

NIH-PA Author Manuscript

NIH-PA Author Manuscript

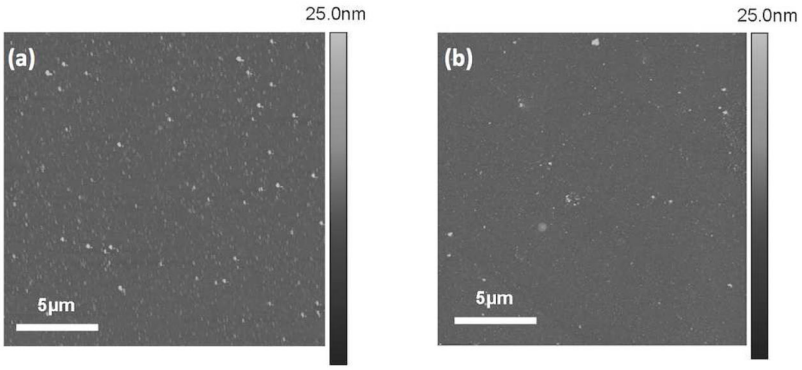

Figure 2.
20μm × 20μm AFM images of (a) an evaporated titanium film on a Si wafer substrate (a) before and (b) after grafting pNaSS.

NIH-PA Author Manuscript
NIH-PA Author Manuscript
NIH-PA Author Manuscript

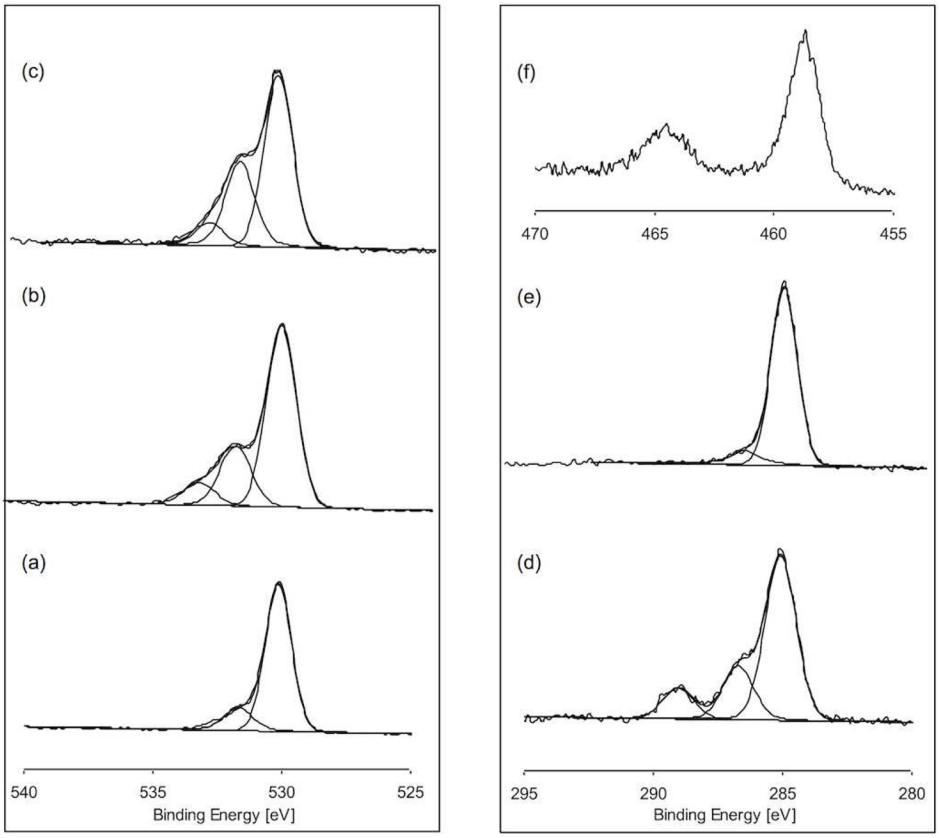

Figure 3.
High-resolution XPS O1s spectra of (a) evaporated titanium, (b) MPS modified titanium and (c) pNaSS grafted titanium. High-resolution XPS C1s spectra of (d) MPS modified titanium and (e) pNaSS grafted titanium. High-resolution XPS Ti2p spectrum of (f) evaporated titanium. The peak assignments for these spectra are provided in Table S1 in the Supporting Information.

NIH-PA Author Manuscript

NIH-PA Author Manuscript

NIH-PA Author Manuscript

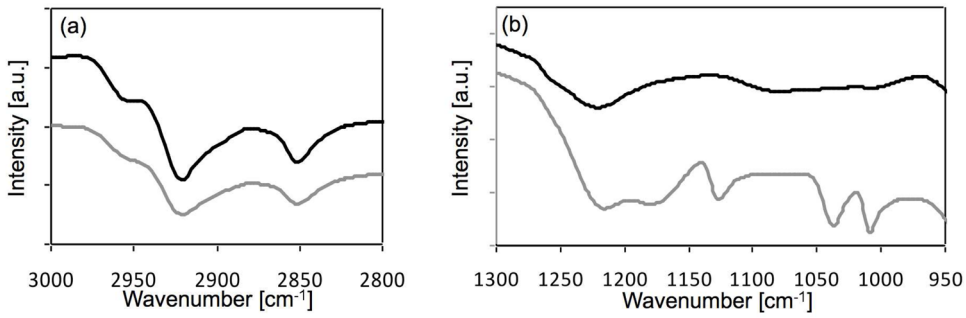

Figure 4.

(a) The FTIR CH region of the MPS modified titanium (black line) and pNaSS grafted titanium (gray line). (b) The FTIR fingerprint region of the pNaSS grafted titanium (grey line) exhibits characteristic peaks from the sulfonate group at 1008 and 1036 cm^{-1} These peaks were not observed on the MPS modified titanium (black line).

NIH-PA Author Manuscript

NIH-PA Author Manuscript

NIH-PA Author Manuscript

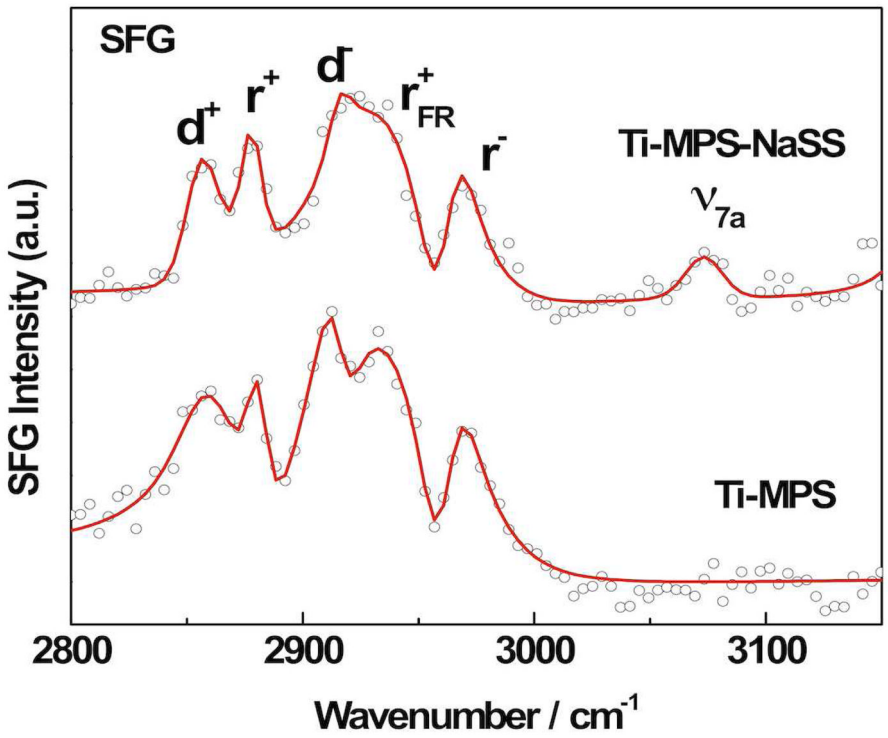

Figure 5.
SFG spectra of MPS modified titanium and pNaSS grafted titanium surfaces. The red line shows a fit of the data using equation 2.

NIH-PA Author Manuscript

NIH-PA Author Manuscript

NIH-PA Author Manuscript

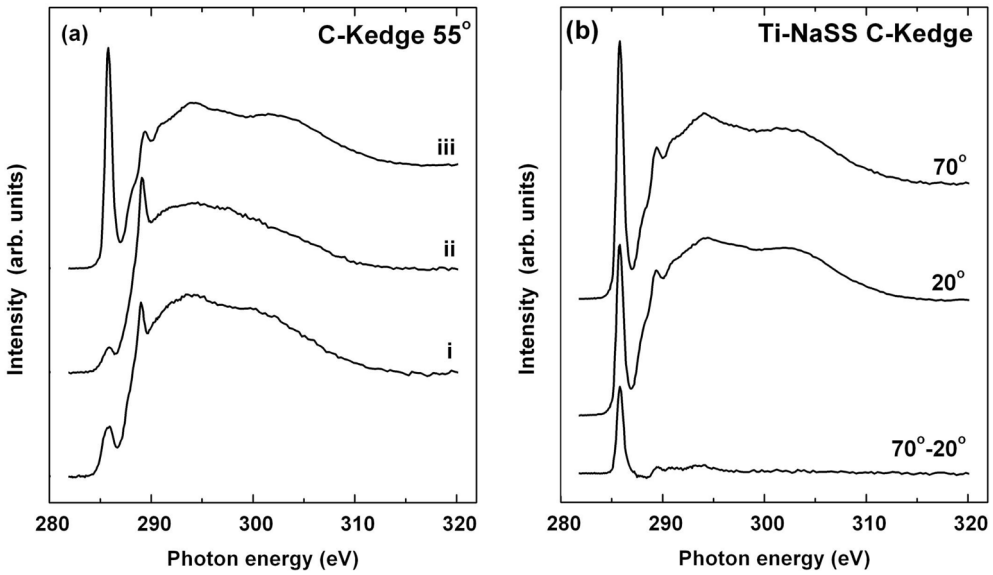

Figure 6.

(a) NEXAFS carbon K-edge spectra acquired at 55° from (i) evaporated titanium, (ii) MPS modified titanium and (iii) pNaSS grafted titanium surfaces. (b) NEXAFS carbon K-edge spectra for the pNaSS grafted titanium surface acquired at 20° and 70°. The difference spectra between the 70° and 20° data is also shown.

NIH-PA Author Manuscript

NIH-PA Author Manuscript

NIH-PA Author Manuscript

Table 1

XPS elemental compositions of: evaporated Ti, MPS modified Ti and pNaSS grafted Ti.

	atomic %		
	Evaporated Ti	**MPS modified Ti**	**pNaSS grafted Ti**
Ti 2p	20.1±0.6	15.2±0.6	8.4±0.2
O 1s	48.5±1.0	50.6±1.0	32.6±0.7
C 1s	31.4±1.6	30.9±1.6	51.1±0.6
Si 2p	---	3.3±0.1	1.3±0.1
Na 1s	---	---	2.2±0.2
S 2p	---	---	3.3±0.1
N1s	---	---	1.1±0.1